Eur. Phys. J. Plus (2018) **133**: 91
DOI 10.1140/epjp/i2018-11948-5

THE EUROPEAN PHYSICAL JOURNAL PLUS

Regular Article

Effect of using guide walls and piers with different geometries on the flow at entrance of a spillway

Matin Jahani[1], Hamed Sarkardeh[2,a], and Ebrahim Jabbari[1]

[1] School of Civil Engineering, Iran University of Science and Technology, Tehran, Iran
[2] Department of Civil Engineering, Faculty of Engineering, Hakim Sabzevari University, Sabzevar, Iran

Received: 20 December 2017 / Revised: 4 February 2018
Published online: 5 March 2018 –

Abstract. In the present paper, the effect of guide wall and pier geometry on the flow pattern of a dam spillway was studied. Different scenarios were numerically simulated to optimize the geometry of the guide walls and piers of the spillway in different hydraulic conditions. The RNG and VOF models were used for turbulence and free surface simulations, respectively. Numerical results were validated with experimental data and good agreement was found with an average relative deviation of less than 10%. Results showed that the vertical inclination of the guide wall and pier was the main affecting factor in the approach flow condition through the spillway. A 44% increase in the vertical inclination of the guide wall resulted in a 43% reduction of the turbulence factor and in a 13% increment of the discharge coefficient of the spillway. By increasing the vertical inclination of the piers of the spillway by 28%, the flow behaviour becomes more uniform and the discharge coefficient increases by as much as 11%. Moreover, the results indicate that increasing the straight length of the guide wall leads to a reduction of the depth-averaged velocity and of the turbulence energy in the approach channel.

1 Introduction

A spillway is a hydraulic structure that is constructed at storage and diversion dams to release surplus water in the reservoir in order to prevent overtopping which could endanger the stability of the dam. To estimate the design discharge of the spillway of a dam, an accurate hydrological process must be performed [1–4]. The inlet flow condition has a significant impact on the spillway performance. At high velocities, vortices appear in the inlet flow, which should be prevented because they lead to the formation of unfavorable approach flow conditions and to the reduction of the discharge capacity. Therefore, a proper inlet channel design is very important and must be hydraulically and structurally adequate in order to provide sufficient capacity [5]. Study of the flow through hydraulic structures is usually conducted by utilization of physical models. This approach is a safe way to analyze the flow through or over hydraulic structures [6–24]. Due to the high cost of laboratory experiments, researchers have attempted to use numerical simulations with physical modeling. In the field of the numerical simulation, the governing equations of the flow, including Navier-Stokes equations and the turbulence models, are solved by numerical methods [25–36]. Some researches were performed on the design of the guide walls over the spillway structure. Jian [37] studied flow conditions according to varying curves of the guide wall. Based on the physical model experiments, Hua and Nan [38] analyzed the optimal layout for a bank spillway. Wang and Chen [5] studied the spillway of the Yutang dam to eliminate the vortex flow and separation on the guide wall. They suggested that the guide wall should be redesigned and they also presented a new shape for the guide wall to eliminate the vortex flow formed at the front of the gate. Martinerie *et al.* [39] experimentally studied the gated spillway of the Shahryar dam in Iran. In their studies, the effect of the vertical inclination of the piers on the flow through the spillway was investigated. Kim *et al.* [40] reviewed the applicability of numerical models to simulate the flow through the spillway. They used the `Flow-3D` model to analyze the flow. Results showed that the flow in approach channel is unstable in the initial design. Therefore, a modified design was suggested. The appropriateness of the modified design was examined by numerical modeling. Their results showed that the flow through the spillway is stable in the modified design. Using a physical model, Rahimzadeh *et al.* [41] studied the effect of the horizontal curvature of the guide walls on the flow over the spillway. Parsaie *et al.* [42] numerically investigated

[a] e-mail: `sarkardeh@hsu.ac.ir`

Fig. 1. Scaled laboratory model of the Jareh dam spillway. Taken from [44].

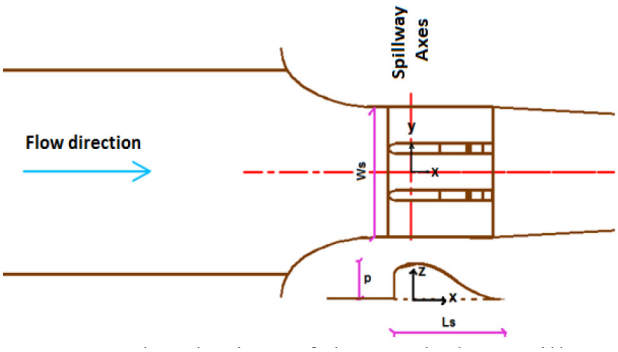

Fig. 2. Sketch view of the Jareh dam spillway.

the influence of the guide walls geometry of the Kamal-Saleh dam spillway on the flow pattern through the approach channel and over the ogee weir. Dehdar-behbahani and Parsaei [43] studied the flow pattern through the guide walls, numerically. Results of their investigation on different turbulence models indicated that the re-normalization group (RNG) model had the best performance on showing the cross waves.

There are few researches on the design and optimization of the guide wall and pier structures over the dam spillways. In the present study, the effect of the guide wall and pier geometries on the flow pattern and rating curve of the dam spillway was studied using a numerical model. To verify the numerical model, experimental data of the flow pattern through the vertical piers and guide walls was used on discharge, flow depths and velocities over the spillway. Then, sensitivity analysis of the grid resolutions in the numerical simulations was performed for the initial model. After verifying the numerical model and considering different scenarios, evaluation of the guide wall and pier geometries was performed in four steps. In each step, the effect of one parameter (straight length of guide wall, horizontal curvatures of end and nose of guide wall, vertical inclination of guide wall and piers) was evaluated, while other parameters were kept constant. In each step, the flow pattern and the rating curve of the spillway were numerically studied in different hydraulic conditions.

2 Materials and methods

Experimental data of the Jareh dam, which is an earth-fill dam, were used to verify the employed numerical model. Figure 1 shows the scaled laboratory model which was developed to study the flow properties through the spillway [44]. The plan view of the gated spillway and the geometric parameters of the designed guide walls are shown in figs. 2 and 3.

In these figures, P represents the height of the spillway upstream face, W_s the spillway width, L_s the length of the spillway, L_c the straight length of the guide wall, R_c and θ_c represent the horizontal core radius and the angle of the guide wall, R_1 and θ_1 the horizontal end radius and the angle of guide wall, R_2 and θ_2 the horizontal nose radius and the angle of the guide wall, t the wall thickness, L_2 and L_1 the top and bottom length of the wall, L_3 the height of the wall, θ_3 the vertical inclination of the wall and θ_4 the vertical inclination of the piers. Analysis of the flow condition shows that the guide wall has a significant effect on the upstream flow condition and optimizing its geometry is the economic way to improve the flow condition [5].

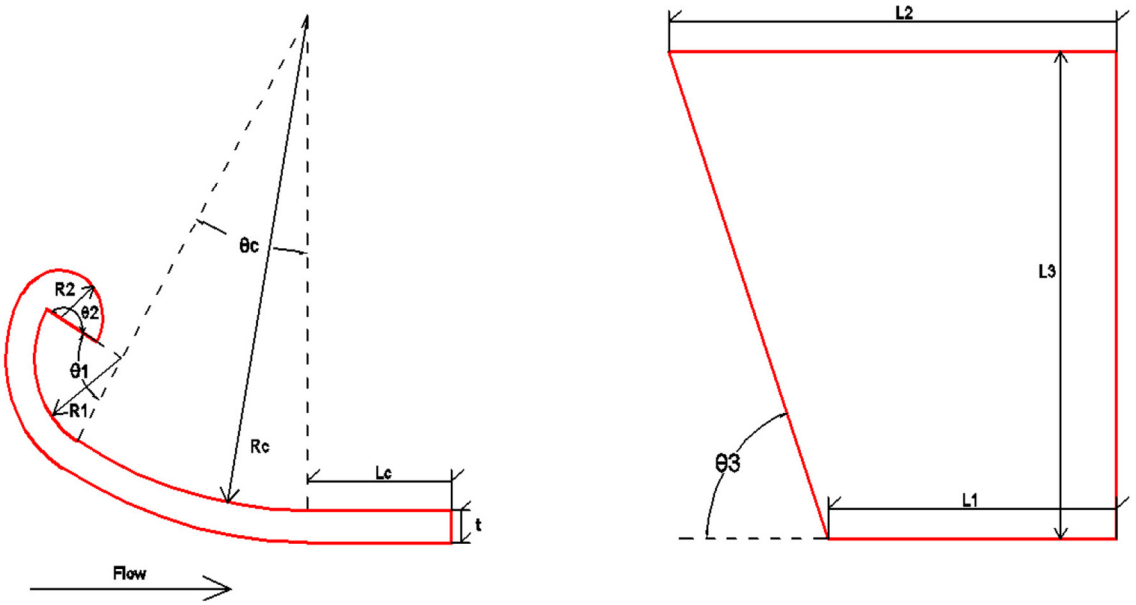

Fig. 3. Geometric parameters of different designed guide walls.

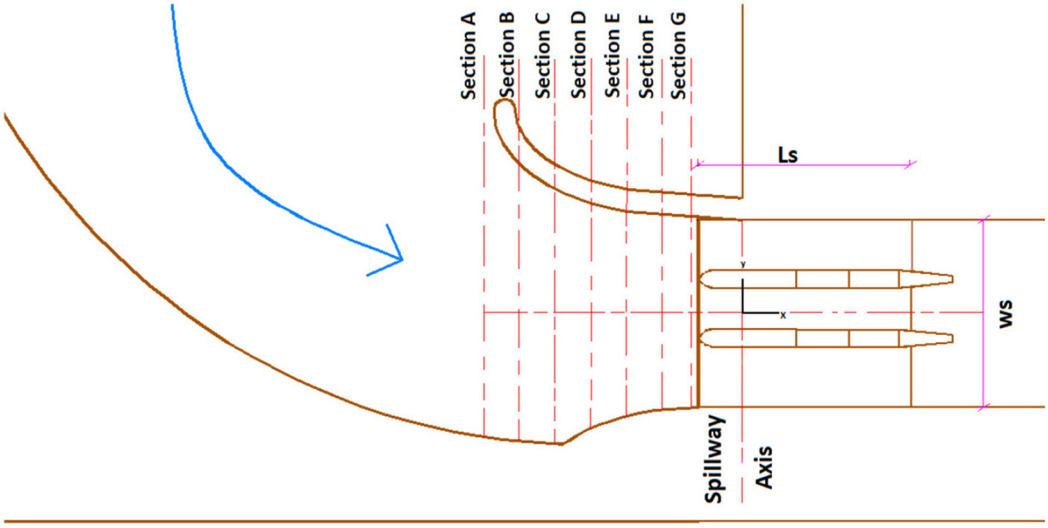

Fig. 4. Plan view of the gated spillway with the curvature of the upstream channel.

A gated spillway, which is oriented at 45° from the axis of the valley, can create a non-uniform approach flow in the bay of the gated spillway. Thus, to assess the effect of the guide wall and pier geometries on the upstream flow properties, the angle between the axis of the spillway and approach channel was assumed to be approximately 45° [39] (fig. 4). To evaluate the geometry of the guide wall and pier, four steps were taken. In each step, the effect of one parameter was evaluated, while other parameters were kept constant. In Step 1, the straight length of the guide wall (L_c), in Step 2, the horizontal curvatures of end and nose of guide wall (R_1, R_2), in Step 3, the vertical inclination of guide wall and finally in Step 4, the vertical inclination of piers were the parameters the effect of which were examined (fig. 5). In each step, optimization of the guide wall was performed at four different water levels ($Z_0/P = 2.11, 2.26, 2.35, 2.56$) in the reservoir. Tables 1, 2, 3 and 4 show the hydraulic and geometric conditions of the wall and piers tested in each step. It should be noted that in all the stages of the study, $R_c = 33\,\mathrm{m}$, $\theta_c = 31°$, $\theta_1 = 90°$, $\theta_2 = 180°$, $t = 2\,\mathrm{m}$ and $L_3 = 30.5\,\mathrm{m}$.

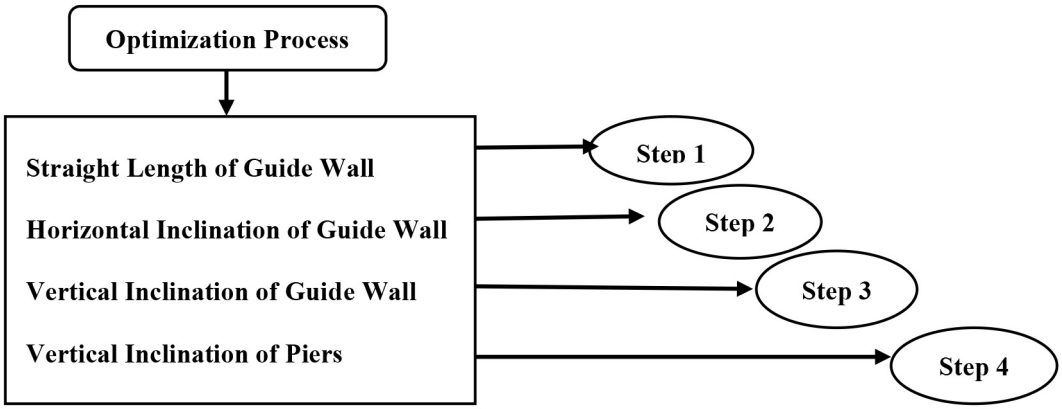

Fig. 5. Simulation steps.

Table 1. Hydraulic and geometric conditions of the guide wall and piers in Step 1.

Alternative	L_c/R_c	Z_0/P				Constant values in each step
1	0.45	2.56	2.35	2.26	2.11	
2	0.30	2.56	2.35	2.26	2.11	$R_1/R_c = 0.24$
3	0.21	2.56	2.35	2.26	2.11	$R_2/R_c = 0.09$
4	0.15	2.56	2.35	2.26	2.11	$\theta_3 = 90^\circ$
5	0.09	2.56	2.35	2.26	2.11	$\theta_4 = 90^\circ$
6	0.00	2.56	2.35	2.26	2.11	

Table 2. Hydraulic and geometric conditions of the guide wall and piers in Step 2.

Alternative	R_1/R_c	R_2/R_c	Z_0/P				Constant values in each step
1	0.36	0.12	2.56	2.35	2.26	2.11	
2	0.30	0.10	2.56	2.35	2.26	2.11	$L_c/R_c = 0.30$
3	0.24	0.09	2.56	2.35	2.26	2.11	$\theta_3 = 90^\circ$
4	0.18	0.07	2.56	2.35	2.26	2.11	$\theta_4 = 90^\circ$
5	0.12	0.06	2.56	2.35	2.26	2.11	

Table 3. Hydraulic and geometric conditions of the guide wall and piers in Step 3.

Alternative	L_1/R_c	θ_3	Z_0/P				Constant values in each step
1	0.96	90°	2.56	2.35	2.26	2.11	$L_c/R_c = 0.30$
2	0.78	80°	2.56	2.35	2.26	2.11	$R_1/R_c = 0.24$
3	0.59	70°	2.56	2.35	2.26	2.11	$R_2/R_c = 0.09$
4	0.37	60°	2.56	2.35	2.26	2.11	$\theta_4 = 90^\circ$
5	0.11	50°	2.56	2.35	2.26	2.11	

Table 4. Hydraulic and geometric conditions of the guide wall and piers in Step 4.

Alternative	θ_4	Z_0/P				Constant values in each step
1	90°	2.56	2.35	2.26	2.11	$L_c/R_c = 0.30$
2	80.8°	2.56	2.35	2.26	2.11	$R_1/R_c = 0.24$
3	70.6°	2.56	2.35	2.26	2.11	$R_2/R_c = 0.09$
4	64.1°	2.56	2.35	2.26	2.11	$\theta_3 = 50^\circ$

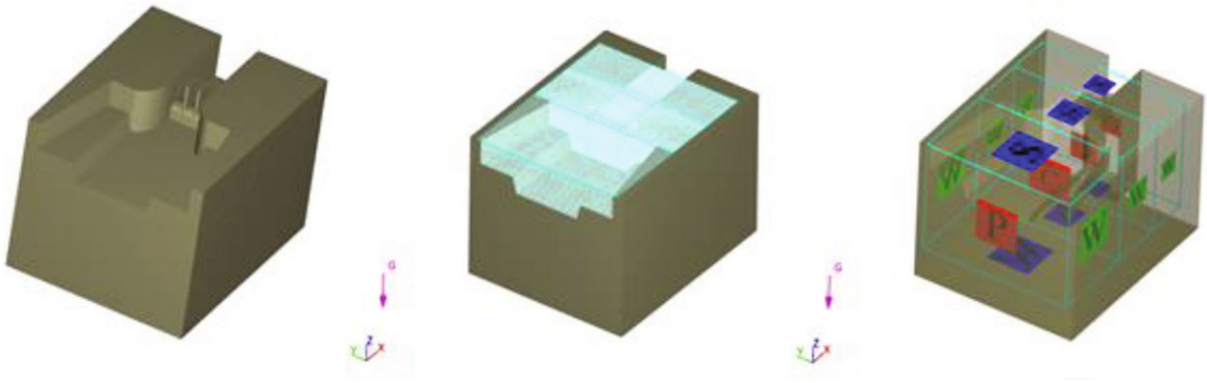

Fig. 6. Sketch of the 3D model of spillway of Jareh dam (a), computational domain of model (b), boundary condition of the model (c).

The equations that govern the fluid flow are continuity and momentum equations, which can be written as

$$\nu_f \frac{\partial \rho}{\partial t} + \frac{\partial}{\partial x}(uA_x) + \frac{\partial}{\partial x}(vA_y) + \frac{\partial}{\partial x}(wA_z) = \frac{PSOR}{\rho}, \tag{1}$$

$$\frac{\partial u}{\partial t} + \frac{1}{\nu_f}\left(uA_x\frac{\partial u}{\partial x} + vA_y\frac{\partial u}{\partial y} + wA_z\frac{\partial u}{\partial z}\right) = -\frac{1}{\rho}\frac{\partial p}{\partial x} + G_x + f_x,$$

$$\frac{\partial v}{\partial t} + \frac{1}{\nu_f}\left(uA_x\frac{\partial u}{\partial x} + vA_y\frac{\partial u}{\partial y} + wA_z\frac{\partial u}{\partial z}\right) = -\frac{1}{\rho}\frac{\partial p}{\partial x} + G_y + f_y,$$

$$\frac{\partial w}{\partial t} + \frac{1}{\nu_f}\left(uA_x\frac{\partial u}{\partial x} + vA_y\frac{\partial u}{\partial y} + wA_z\frac{\partial u}{\partial z}\right) = -\frac{1}{\rho}\frac{\partial p}{\partial x} + G_z + f_z, \tag{2}$$

where, x, y and z denote the Cartesian coordinates, u, v and z are the mean velocity vectors, A_x, A_y and A_z are the cross-sectional area of the flow, ρ is the fluid density, PSOR is the mass source term, ν_f is the volume fraction of the fluid, P is the fluid pressure, G_x, G_y and G_z are the acceleration created by the body forces and f_x, f_y and f_z are the components of the acceleration due to the viscosity.

Based on the volume fraction of the computational cells, the volume of fluid (VOF) technique was employed to model the free surface profile [25,45–47]. F, the amount of fluid in each cell, takes a value between 0 and 1,

$$\frac{\partial F}{\partial t} + \frac{1}{\nu_f}\left[\frac{\partial}{\partial x}(FA_x u) + \frac{\partial}{\partial y}(FA_y v) + \frac{\partial}{\partial z}(FA_z w)\right] = 0. \tag{3}$$

The RNG turbulence model is a powerful turbulence model which has suitable performance to model flow over spillways [28]. The equations mostly used in the RNG turbulence model are given as follows:

$$\frac{\partial}{\partial t}(\rho k) + \frac{\partial}{\partial x}(\rho u_i k) = \frac{\partial}{\partial x_i}\left(\alpha_k \mu_{eff}\frac{\partial k}{\partial x_i}\right) + G_k + G_b - \rho\varepsilon, \tag{4}$$

$$\frac{\partial}{\partial t}(\rho \varepsilon) + \frac{\partial}{\partial x}(\rho u_i \varepsilon) = \frac{\partial}{\partial x_i}\left(\alpha_k \mu_{eff}\frac{\partial \varepsilon}{\partial x_i}\right) + C_{1\varepsilon}\frac{\varepsilon}{k}(G_k + C_{3\varepsilon}G_b) - C_{2\varepsilon}\rho\frac{\varepsilon^2}{k} - R, \tag{5}$$

where G_k is the rate of the kinetic energy creation and R is the turbulence density defined as

$$R = \frac{C_\mu \rho \eta^3 (1 - \eta/\eta_0)}{1 + \beta\eta^3}\frac{\varepsilon^2}{k}, \qquad \mu_t = \rho C_\mu \frac{k^2}{\varepsilon}, \tag{6}$$

in which $\beta = 0.012$, $\eta_0 = 1.38$. The entire geometrical domain in (x, y, z) had the dimensions of $145 \times 120 \times 110.5$ m (fig. 6(a)). The mesh grid was composed of three different mesh blocks with cubic cells (fig. 6(b)). The boundary conditions were specified by pressure at the entrance of the channel through the definition of the corresponding water levels, outflow downstream of the chute and continuity between mesh blocks (fig. 6(c)).

In fig. 6, W is the wall, P the specified pressure, S the symmetry, O the outflow and C the continuative boundary conditions.

Table 5. Cell sizes for each simulation in the grid sensitivity analysis.

Simulation	Mesh block 1	Mesh block 2	Mesh block 3
1	2	1	1.2
2	1.75	0.75	1
3	1.5	0.6	0.75
4	1.25	0.5	0.6

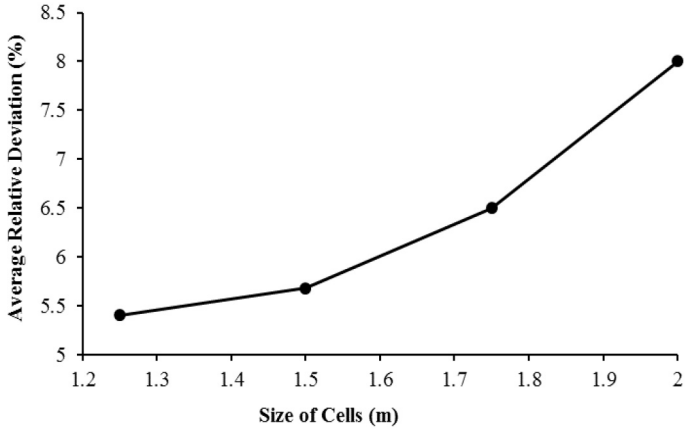

Fig. 7. Deviation of the simulations *versus* sizes of cubic cell in Mesh block 1.

2.1 Grid sensitivity analysis

To specify the mesh independency in this study, four numerical simulations were performed with different mesh sizes (table 5). In each simulation, the flow depth was recorded in the middle of the symmetric part of the channel and was compared with the experimental data. The total deviation *versus* the size of the cubic cells is plotted and shown in fig. 7.

As is shown in fig. 7, the total deviations decreased and improved from simulation 1 to simulation 3, so, there is no need to make cell sizes any smaller, because changes of total deviations from simulation 3 to simulation 4 were not considerable. Consequently, simulation 3, with cell sizes of 1.5 m for mesh block 1, 0.6 m for mesh block 2 and 0.75 m for mesh block 3 had the best grid sizes. As is shown in fig. 7, the numerical results were found to be in good agreement with the measured values with an average relative deviation of less than 10%.

2.2 Prediction of the accuracy of the flow depth and the depth-averaged velocity

Figure 8 compares the flow depth and the depth-averaged velocity obtained from the numerical modeling (the RNG turbulence model and the cell sizes of simulation 3 in table 5) with the measured values.

The agreement between the results of the numerical analyses and those obtained by the experiments was appropriate. The average deviation between the results of the simulation and the measured values for flow depth and velocity was approximately 5% and 8%, respectively. In fig. 8, Z is the flow depth, X the distance from ogee spillway and V_0 the inlet velocity. According to the verification results and by comparing the flow depth and depth-averaged velocity of the numerical model and simulation, it is concluded that the numerical model can be used to evaluate flow conditions.

3 Results and discussions

3.1 The effect of the straight length of the guide walls on the approach flow in Step 1

The effect of the straight length of the guide wall was studied by taking six values for the length ($L_c/R_c = 0.45, 0.30, 0.21, 0.15, 0.09$). Figure 9 shows the guide walls with different lengths.

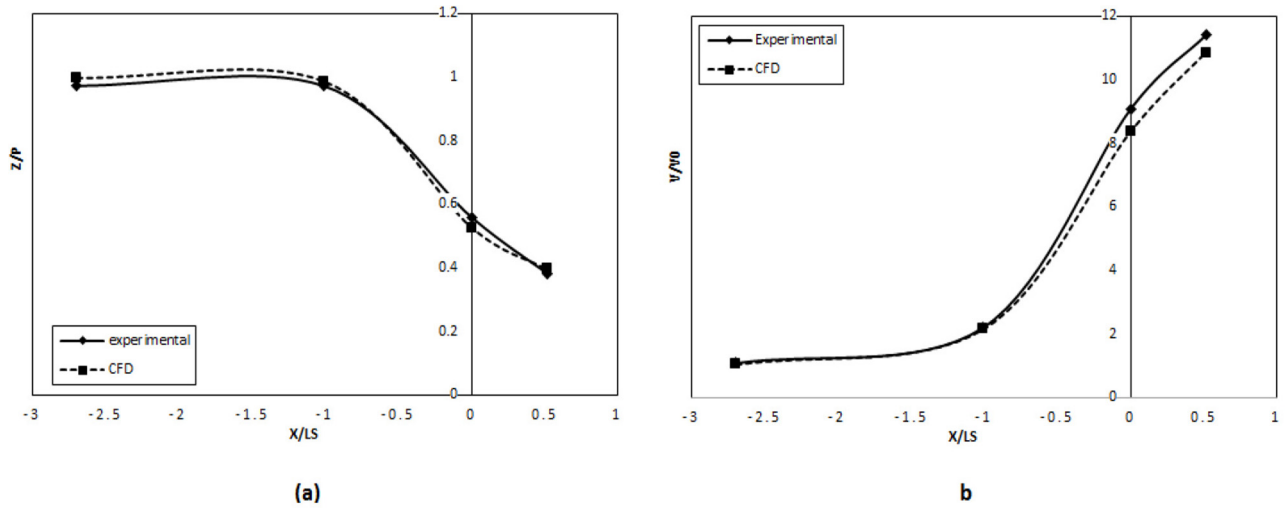

Fig. 8. Comparison of flow depth (a) and the depth-averaged velocity (b) as obtained by CFD analysis and experiment.

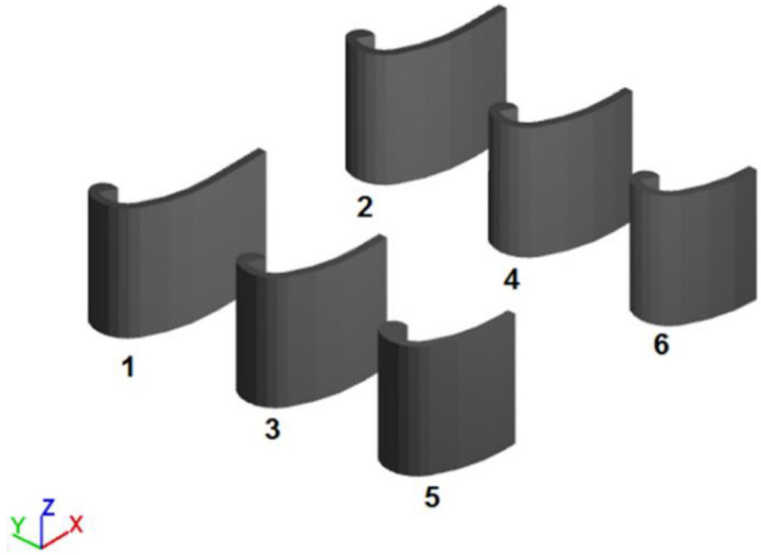

Fig. 9. Guide walls used in the numerical model with different lengths.

3.2 The distributions of the turbulent kinetic energy (k)

Figure 10 shows the effect of the length of the guide wall on the turbulent kinetic energy (k) at $X/L_s = -0.715$ and fig. 11 shows the distributions of the turbulent kinetic energy (k) for different length of the guide wall at $Z_0/P = 2.56$.

The peak value of k occurs near the guide wall for all the different lengths of the guide wall. By increasing the length of the guide wall from $L_c/R_c = 0.0$ to $L_c/R_c = 0.30$, the values of the turbulent energy decreases and then increases again. The decrement of maximum turbulent energy compared to $L_c/R_c = 0.00$ in $L_c/R_c = 0.09, 0.15, 0.21, 0.30$ and 0.45 was 3%, 6%, 9%, 21% and 15%, respectively, because, by increasing the length of the guide wall the flow stablizes more and, as a result, turbulence energy decreases. By increasing the length of the wall from $L_c/R_c = 0.30$ to $L_c/R_c = 0.45$, turbulence energy increases due to the reduction of the effective width of the inlet flow towards the spillway.

3.3 Distributions of the depth-averaged velocity in the approach channel

Figure 12 shows the effect of the length of the guide wall on the depth-averaged velocity along the approach channel and fig. 13 shows the distributions of the depth-averaged velocity for different length of the guide wall at $Z_0/P = 2.56$.

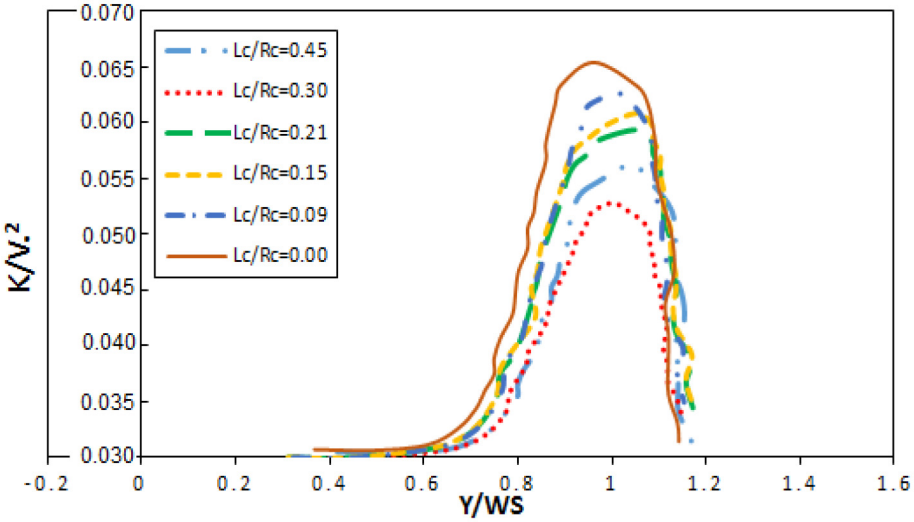

Fig. 10. Turbulent kinetic energy *versus* different length of the guide wall at $X/L_s = -0.715$.

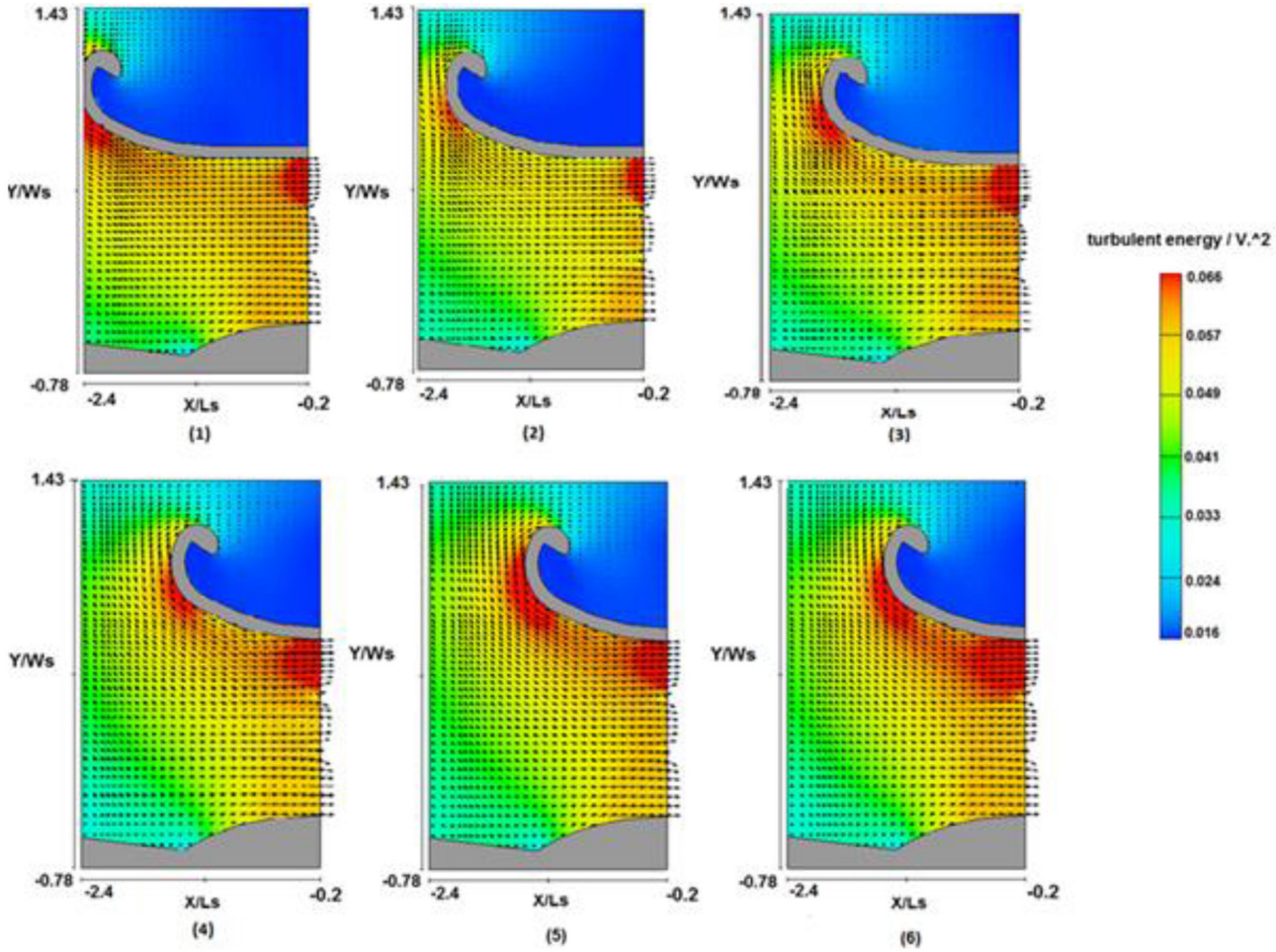

Fig. 11. Distributions of the turbulent kinetic energy for different lengths of the guide wall in the approach channel.

By increasing the length of the guide wall, the values of the velocity became smaller. The decrement of the depth-averaged velocity near the spillway at $L_c/R_c = 0.09, 0.15, 0.21, 0.30$ and 0.45 was 2%, 9%, 22%, 30% and 39%, respectively (compared to $L_c/R_c = 0$). This may be due to the increase of friction between the flow and the guide wall which extends far into the approach channel thus, causing a reduction in the depth-averaged velocity.

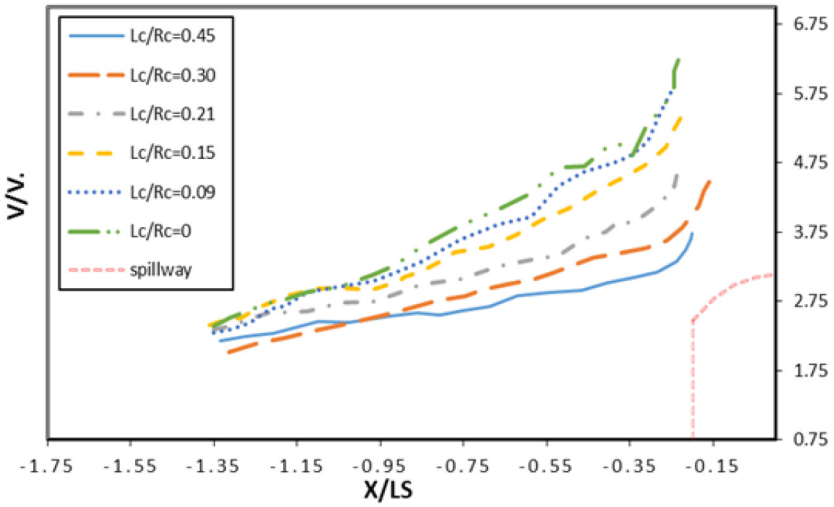

Fig. 12. Depth-averaged velocity *versus* different length of the guide wall in the approach channel.

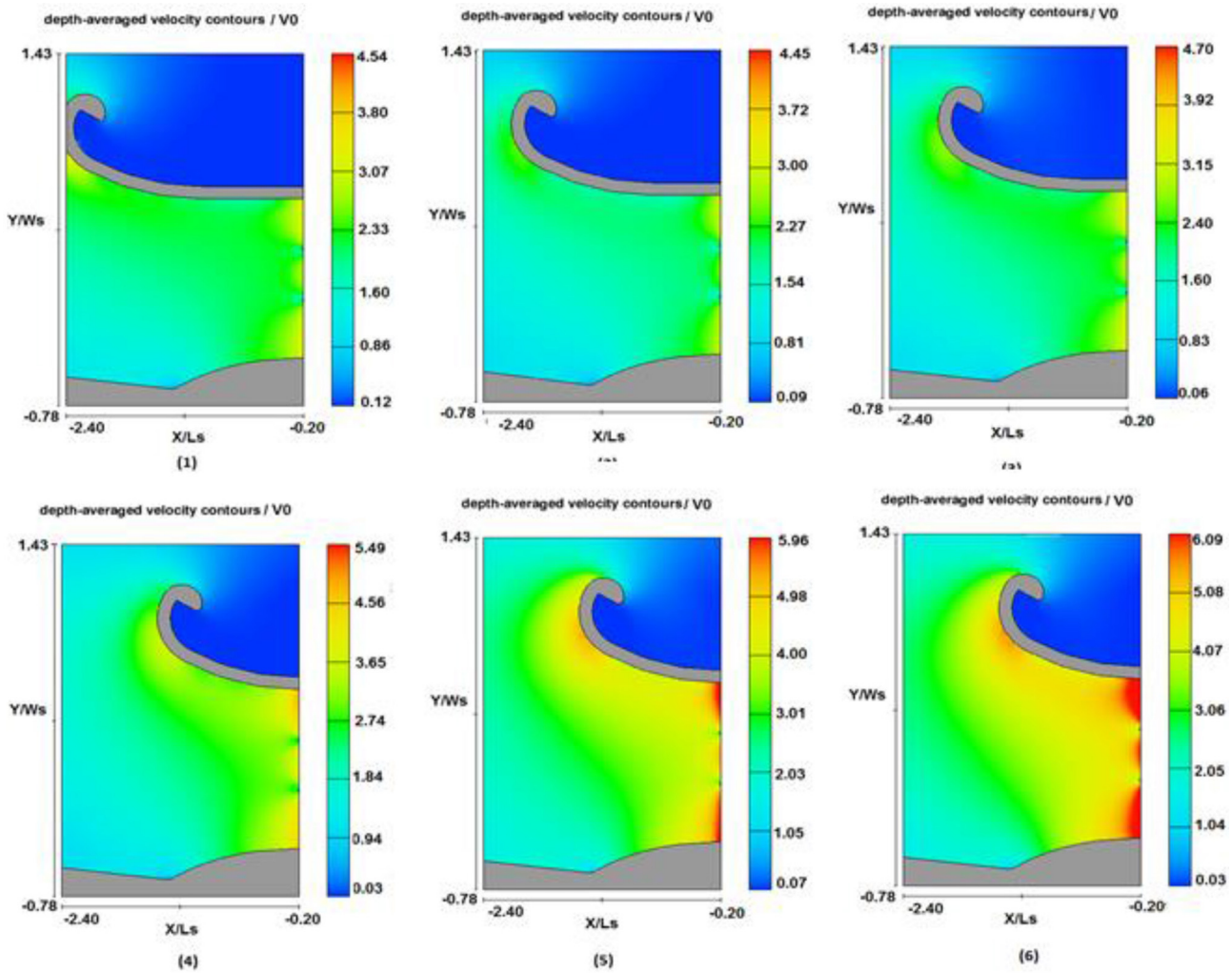

Fig. 13. Distributions of the depth-averaged velocity for different length of the guide wall in the approach channel.

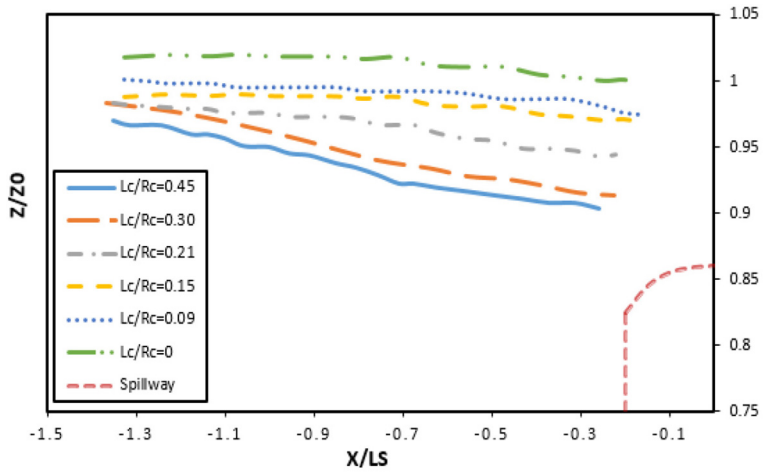

Fig. 14. Flow depth *versus* different lengths of the guide wall in the approach channel.

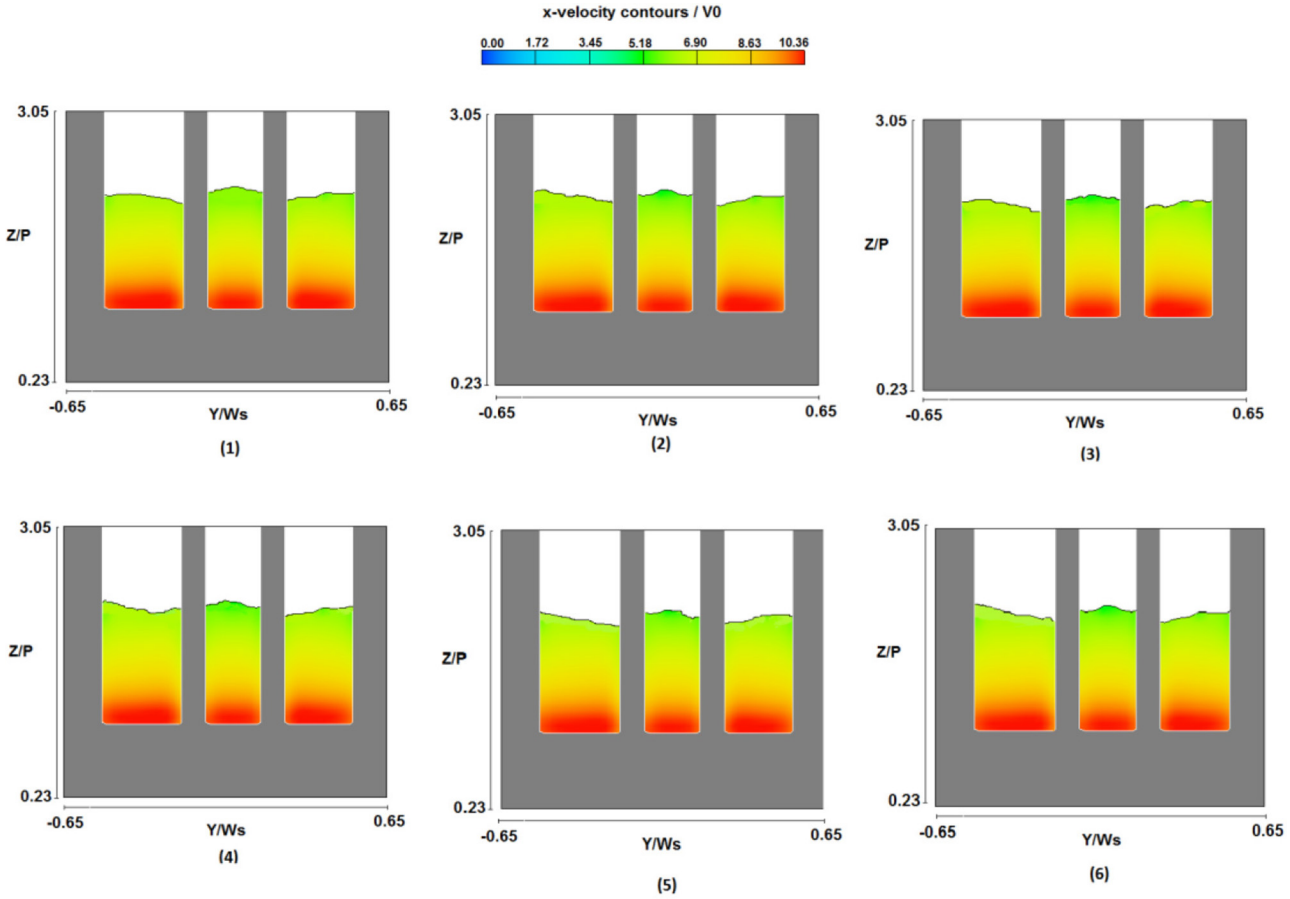

Fig. 15. Cross-section of the flow through the spillway for different lengths of the guide wall.

3.4 Distributions of the flow depth in the approach channel

Figure 14 shows the effect of the length of the guide wall on the flow depth along the approach channel and fig. 15 shows the cross-section of the flow through the spillway for different length of the guide wall at $Z_0/P = 2.56$.

Increasing the length of the guide wall leads to the reduction of the flow depth values. The decrement of the flow depth near the spillway compared to $L_c/R_c = 0$ for $L_c/R_c = 0.09$, 0.15, 0.21, 0.30 and 0.45 was 2.8%, 4%, 6.2%, 7% and 8.5%, respectively. By decreasing the length of the guide wall, the turbulent energy near the wall increases and by contraction of the flow near the wall the flow depth declines. As a result, the flow depth increases in the central axis and the flow becomes less uniform. As can be seen in fig. 15, increasing the length of the guide wall leads to smoother flow passing with less cross wave creation.

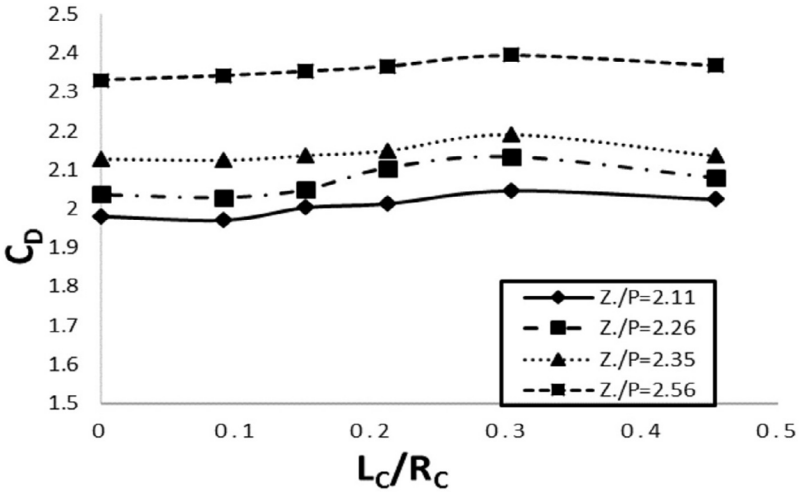

Fig. 16. Discharge coefficient of the spillway for different straight lengths of the guide wall.

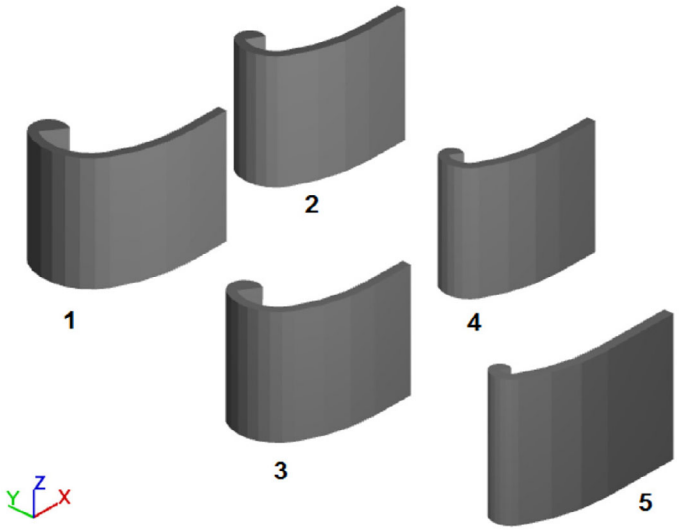

Fig. 17. Guide walls used in the numerical model with different horizontal curvatures.

3.5 Effect of the straight length of the guide wall on the discharge coefficient

The hydraulic capacity Q of a free crest spillway is classically computed as

$$Q = C_d \cdot b_e \cdot \sqrt{2g} \cdot H^{\frac{3}{2}}, \tag{7}$$

where C_d is the discharge coefficient, b_e the effective width, g the gravitational acceleration and H the upstream hydraulic head. The effective width allows the lateral flow contraction to be taken into account. It can be expressed as

$$b_e = b - (2 \cdot n \cdot k_p + k_a) \cdot H, \tag{8}$$

where b is the total width of the bays, n the number of the piers and k_p and k_a the contraction factors for the piers and abutment, respectively. Contraction factors for the piers and the walls have been determined experimentally as constant values of 0.05 and 0.2 [48].

Comparison of the discharge coefficient with different length of the guide wall, and with different water level in the reservoir showed that the wall with $L_c/R_c = 0.30$ allows the maximum evacuated discharge. Figure 16 shows the discharge coefficient *versus* the straight length of the wall. Increasing the length of the wall from $L_c/R_c = 0.00$ to $L_c/R_c = 0.30$ results in a 4% increase in the discharge coefficient.

3.6 Effect of horizontal inclination of guide walls on approach flow to spillway in Step 2

The effect of the horizontal inclination of the guide walls on the flow is studied, for five different inclinations ($R_1/R_c = 0.12, 0.18, 0.24, 0.30, 0.36$), in this section and shown in fig. 17.

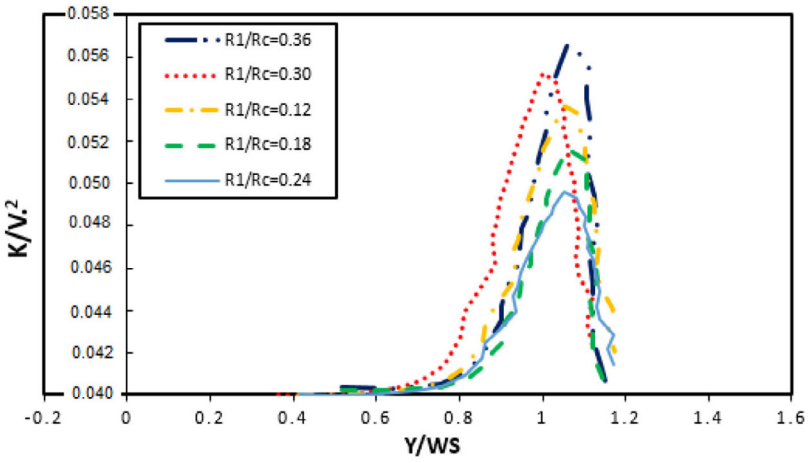

Fig. 18. Turbulent kinetic energy *versus* different horizontal radii of the guide wall at $X/L_s = -2.23$.

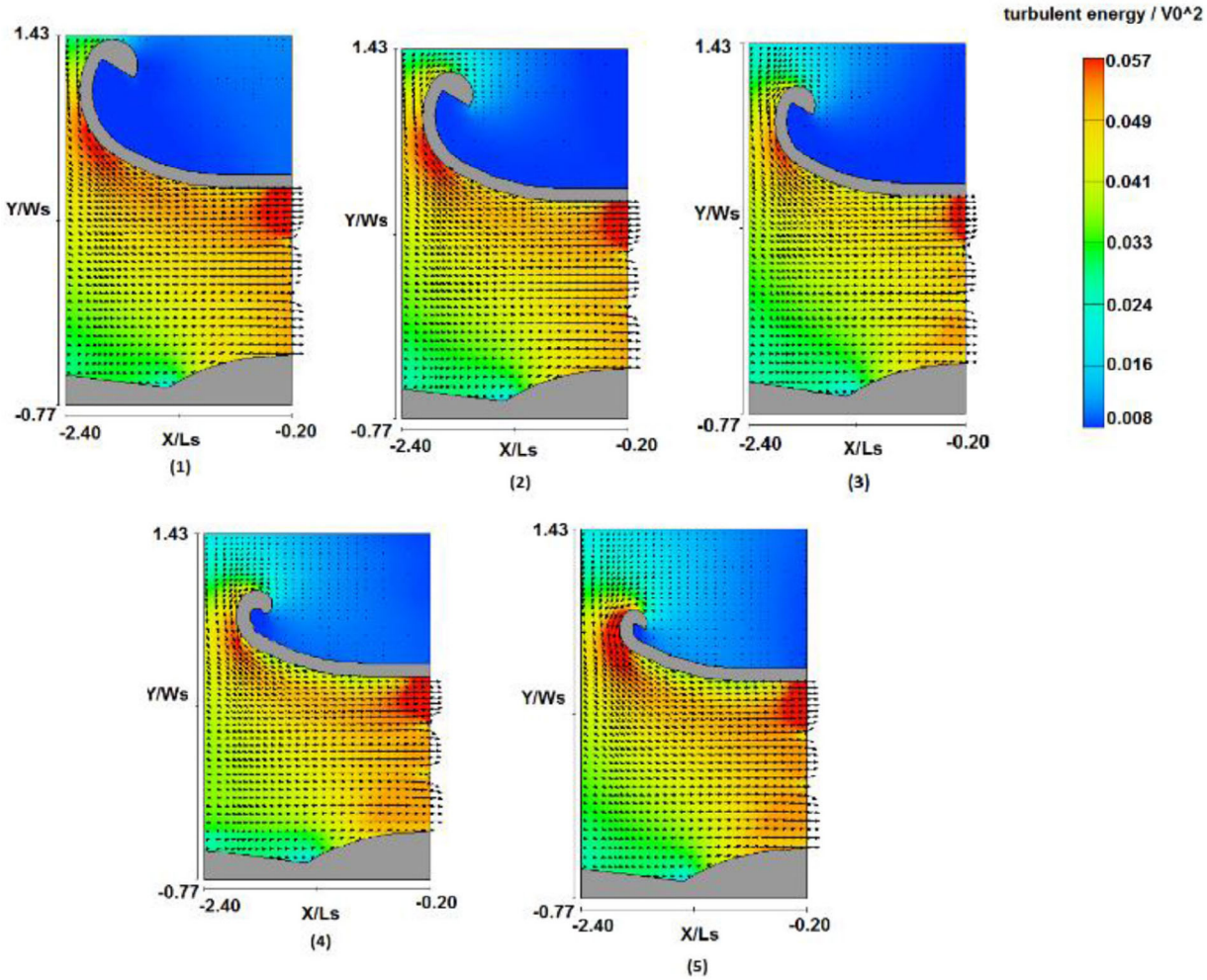

Fig. 19. Distributions of the turbulent kinetic energy of the flow in the approach channel for different horizontal radii of the guide wall.

3.7 Distribution of turbulent energy k in different horizontal curvatures

Figure 18 compares the turbulent kinetic energy k for different horizontal radii of the guide wall at $X/L_s = -2.23$ and fig. 19 shows the distribution of the turbulent kinetic energy k for different horizontal radii along the approach channel.

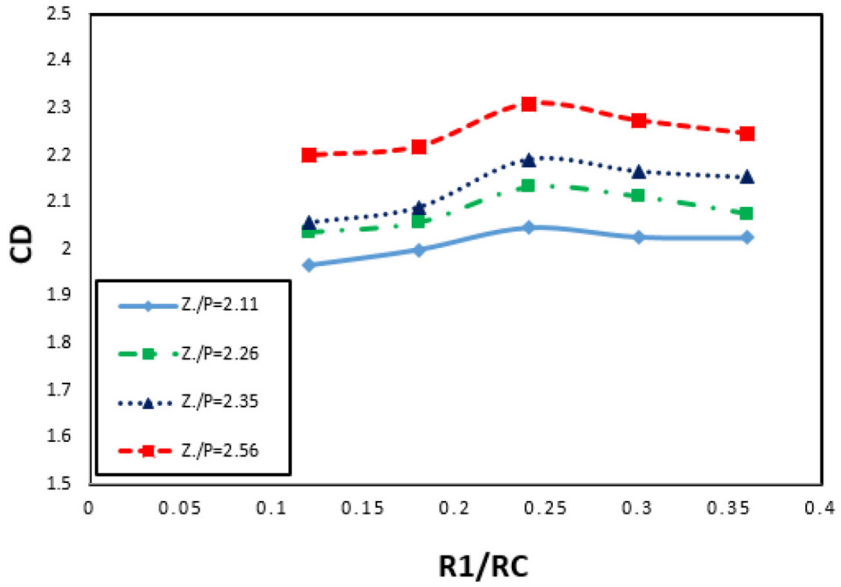

Fig. 20. Discharge coefficient of the spillway for different horizontal curvatures of the guide wall.

The peak value of k occurs near the guide wall for all the curvatures. With $R_1/R_c = 0.24$, the amount of the turbulent energy is the lowest ($K/V_0^2 = 0.0495$). The turbulent energy in the approach channel is influenced by the adjustment of the wall bend to the curvatures of the flow lines. On the other hand, optimal values of the horizontal inclination of the guide wall are affected by the topography of the approach channel, the angle between the axis of the approach channel and that of the spillway. Therefore, based on the experimental data, the guide wall with $R_1/R_c = 0.24$ is the one with the best horizontal inclination.

3.8 Effect of horizontal inclination of the guide wall on the discharge coefficient

Comparison of the experimental results shows that for different horizontal inclinations of the guide wall and varying water level in the reservoir, the wall with $R_1/R_c = 0.24$ allows the greatest spillway discharge. By increasing the horizontal inclination from 0.12 to 0.24, the discharge coefficient increases by 4%. Figure 20 shows the discharge coefficient *versus* the horizontal inclination of the wall.

3.9 Effect of the vertical inclination of the guide wall on the approach flow to spillway in Step 3

By using movable and flexible elements, the research for the optimal shape indicates that a vertical inclination of the nose of the guide wall leads to an improvement of the approach flow condition. The nose inclination of the walls acts as the prow of a ship and, as a result, contributes to a better flow distribution. Consequently, the separation zone was no more concentrated on one vertical line. The effect of the vertical inclination of the guide wall was studied by using five inclinations ($\theta = 90°$, $80°$, $70°$, $60°$, $50°$). Figure 21 shows guide walls geometry.

3.10 Distribution of the turbulent energy k for different vertical inclinations of the guide wall

Figure 22 shows the effect of the vertical inclination of the guide wall on the turbulent kinetic energy and fig. 23 shows the distribution of the turbulent kinetic energy k for different vertical inclinations of the guide wall along the approach channel.

The turbulent energy decreases as the vertical inclination increases. Figure 22 shows that by increasing the vertical inclination by 44%, the maximum turbulent energy decreases by 43%. In fact, with a smaller vertical inclination a greater velocity gradient is expected and the turbulent energy increases as a result of a greater velocity gradient.

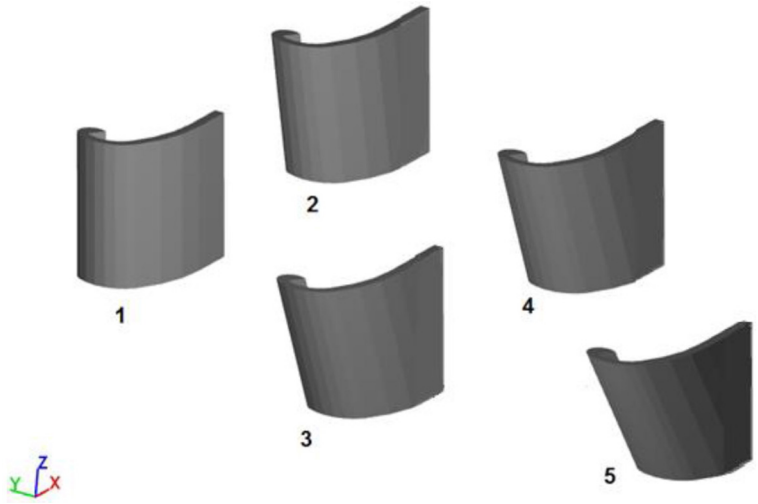

Fig. 21. Guide walls used in the numerical model with different vertical inclinations.

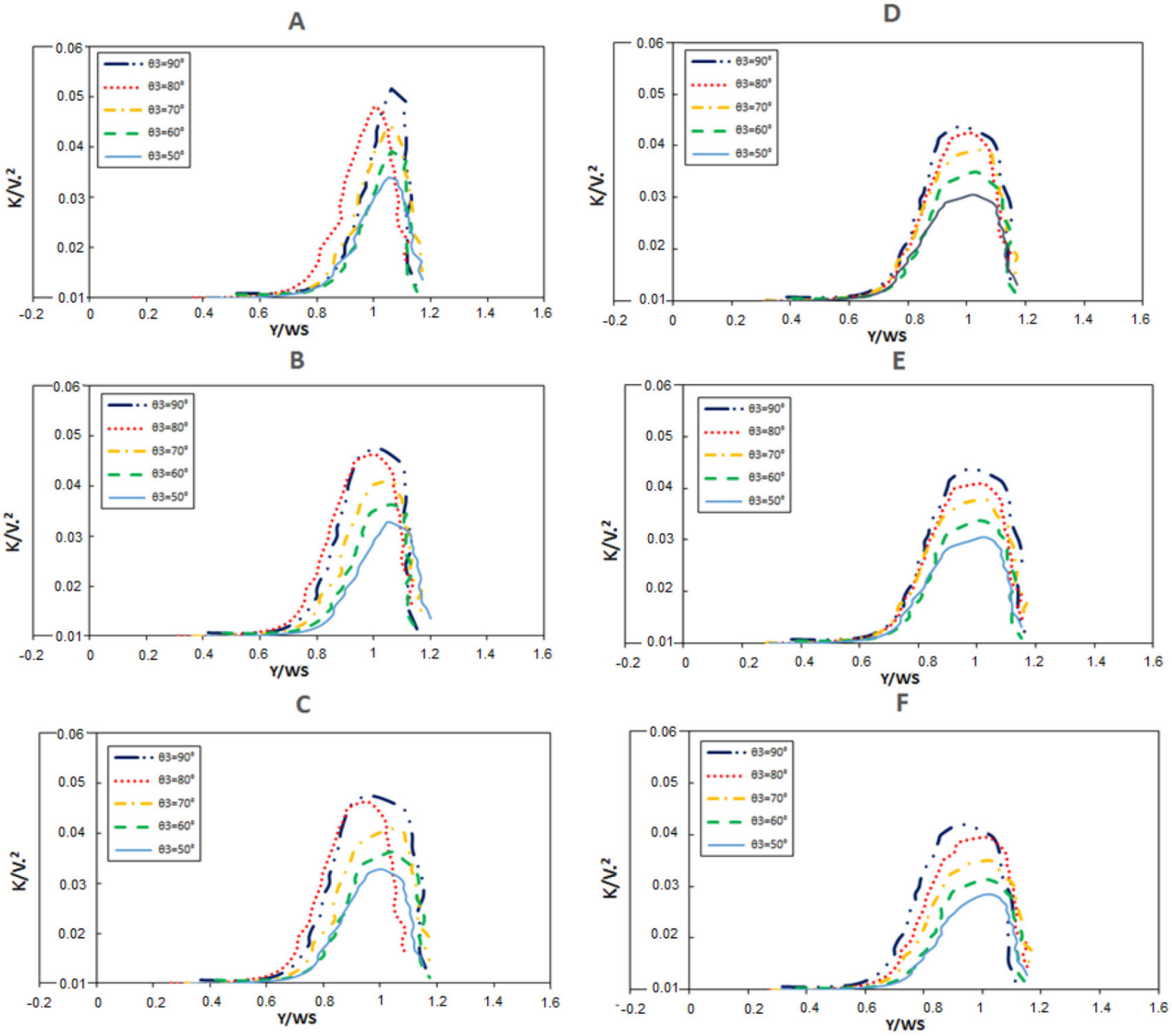

Fig. 22. Turbulent kinetic energy *versus* different vertical inclination of the guide wall at sections A, B, C, D, E and F.

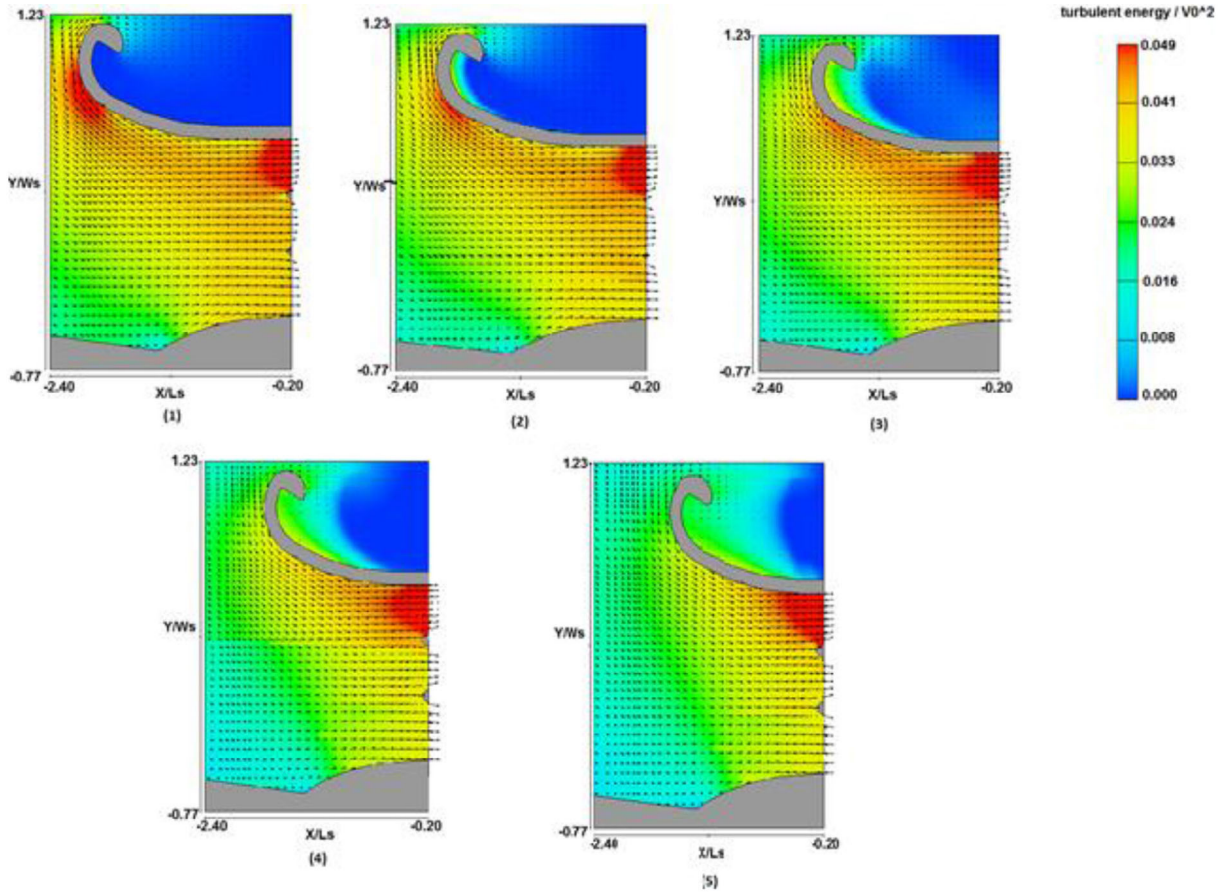

Fig. 23. Distributions of the turbulent kinetic energy for different vertical inclinations of the guide wall in the approach channel.

3.11 Distributions of the depth-averaged velocity in the approach channel

The effect of the vertical inclination of the guide wall on the depth averaged velocity at sections A, B, C, D, E and F (fig. 4) was evaluated. Figure 24 shows the distribution of the depth-averaged velocity for different vertical inclinations of the guide wall along the approach channel.

As is shown in figs. 24 and 25, by increasing the vertical inclination of the walls, the depth-averaged velocity in the approach channel decreases. For example, in fig. 24(F), for section F, the depth-averaged velocity decreases by 4%, 9%, 10% and 13% for the 80°, 70°, 60° and 50° vertical inclination, respectively.

3.12 Distributions of the flow depth in the approach channel

Figure 26 compares the distribution of the flow depth for different vertical inclinations of the guide wall and fig. 27 shows the cross-section of the flow through the spillway for different vertical inclinations of the guide wall at $Z_0/P = 2.56$. The values of the flow depth become smaller as the vertical inclination of the guide wall decreases. The water level drops near the spillway for $\theta_3 = 90°$, 80°, 70°, 60° and 50° as 10%, 7%, 6%, 5% and 4%, respectively. As can be seen in fig. 27, increasing the vertical inclination of the guide wall leads to a smoother flow passing with a less cross wave creation.

3.13 Effect of the vertical inclination of the guide wall on the discharge coefficient

Figure 28 shows the variation of the discharge coefficient of the spillway for different vertical inclinations of the guide wall for different water levels in the reservoir.

As can be seen from fig. 28, with $\theta_3 = 50°$ as the angle of the inclination of the guide wall or with a 44% increase of inclination, the discharge capacity and consequently the discharge coefficient increase by as much as 12.9%.

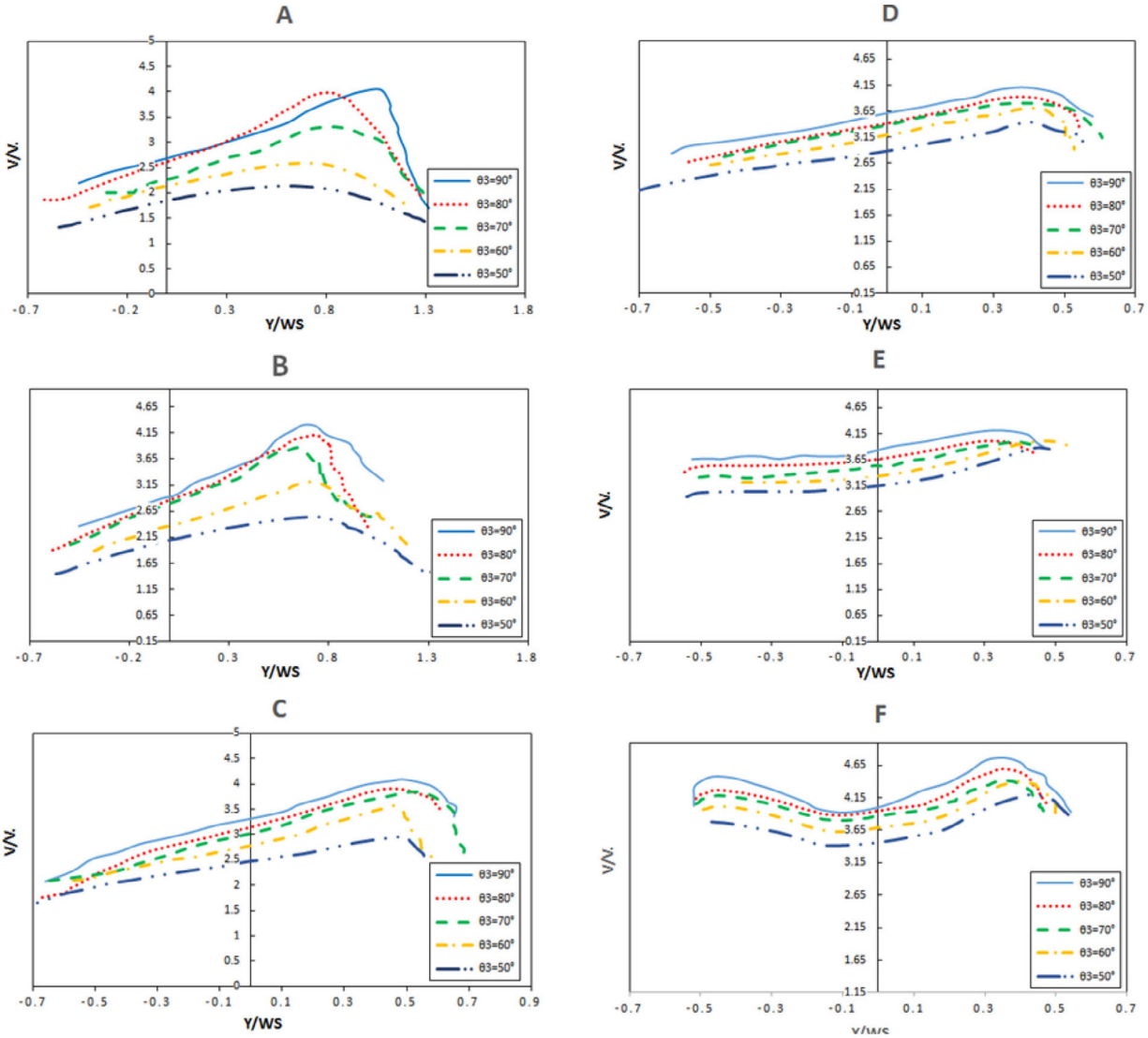

Fig. 24. Depth-averaged velocity *versus* different vertical inclinations of the guide wall at sections A, B, C, D, E and F.

3.14 Effect of the vertical inclination of the piers on the flow to spillway in Step 4

Results show that a longitudinal inclination of the nose of the piers improves the approach flow condition. In this study, four inclinations of the piers ($\theta = 90°$, 80.8°, 70.6°, 60.1°) were examined (fig. 29). Figure 30 shows the cross-section of the flow through the spillway for different vertical inclinations of the piers at $Z_0/P = 2.56$. As is shown in fig. 30, by increasing the vertical inclination of piers, the flow becomes smoother and less cross wave is created.

3.15 Effect of the vertical inclination of the piers on the discharge coefficient

Figure 31 shows the discharge coefficient of the spillway for different vertical inclinations of the piers.

Comparison of the results of the simulations with different inclinations of the piers and with different water levels in the reservoir shows that the wall with an inclination of $\theta_3 = 64.1°$ allows the maximum evacuated discharge. Figure 31 shows the variation of the discharge coefficient *versus* the vertical inclination of the piers. By a 28% increase in the inclination of the piers, the discharge coefficient increases by 11%. By applying longitudinal inclination to the nose of the piers, the flow passes more uniformly through the bays of the spillway and, by improving the symmetry of the spillway flow, the discharge coefficient increases. Also, as the water level increases in the reservoir, the discharge coefficient becomes greater and greater, and this happens due to the velocity distribution in the channel depth (more uniform velocity distribution).

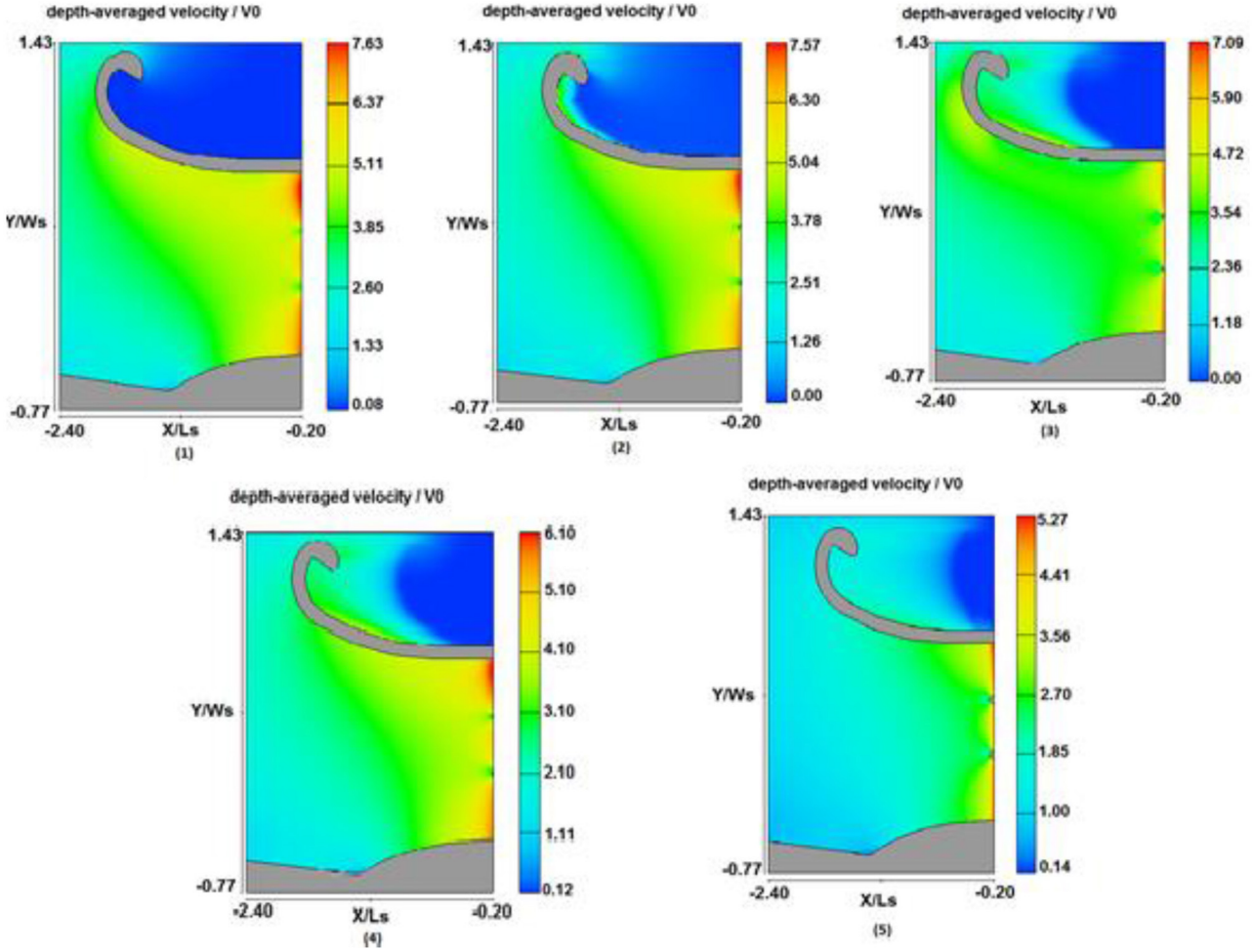

Fig. 25. Distributions of the depth-averaged velocity for different vertical inclinations of the guide wall in the approach channel.

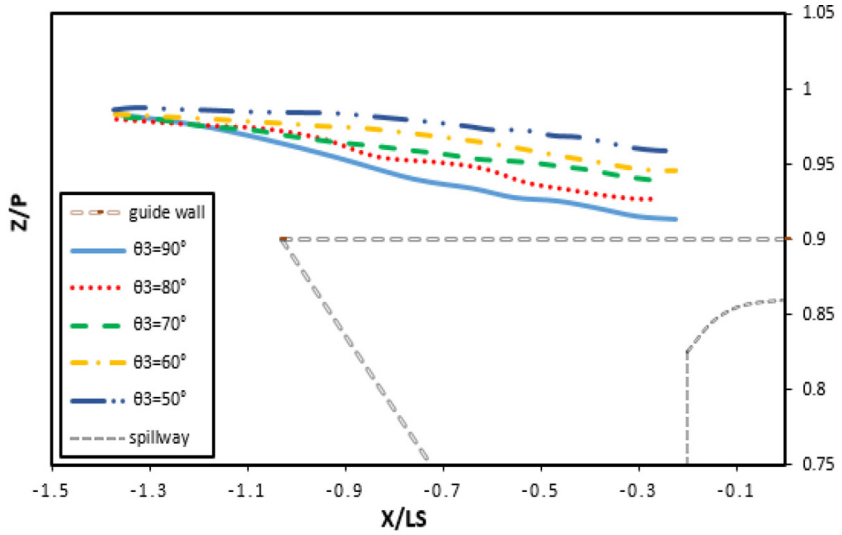

Fig. 26. Flow depth *versus* different vertical inclination of the guide wall in the approach channel.

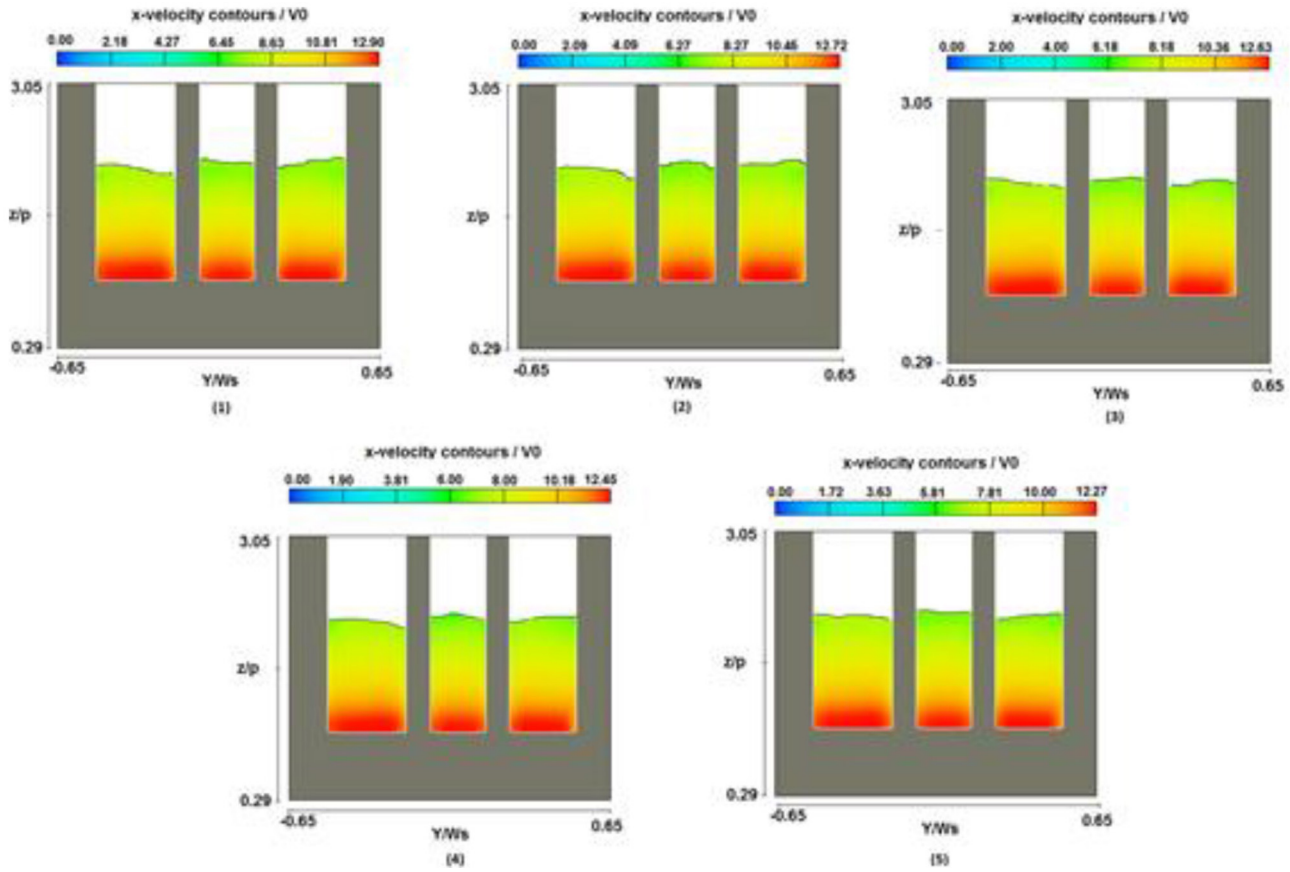

Fig. 27. Cross-section of the flow through the spillway for different vertical inclinations of the guide wall.

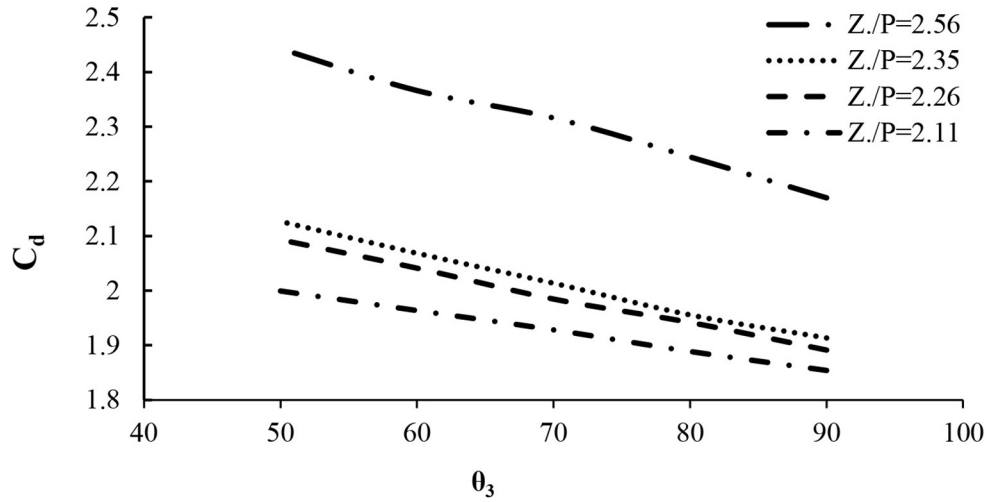

Fig. 28. Discharge coefficient of the spillway for different vertical inclinations of the guide wall.

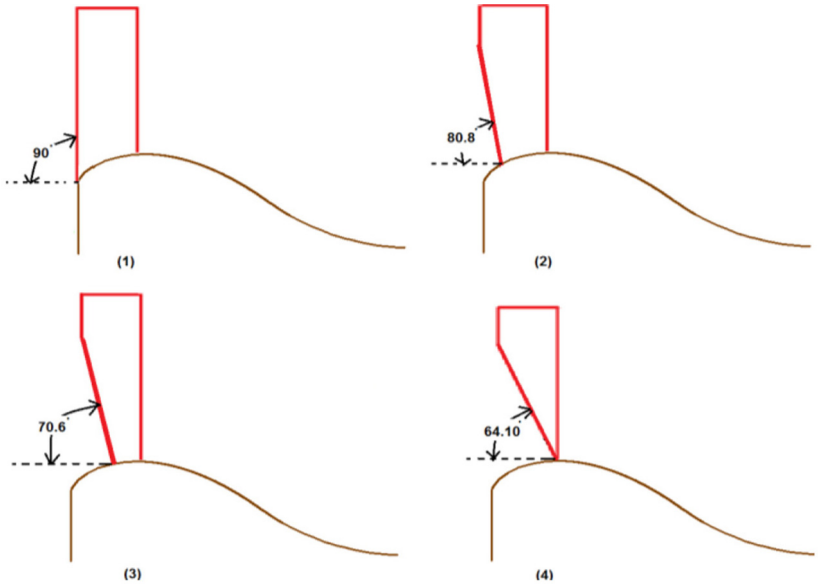

Fig. 29. Sketch of the piers in the numerical model with different vertical inclinations.

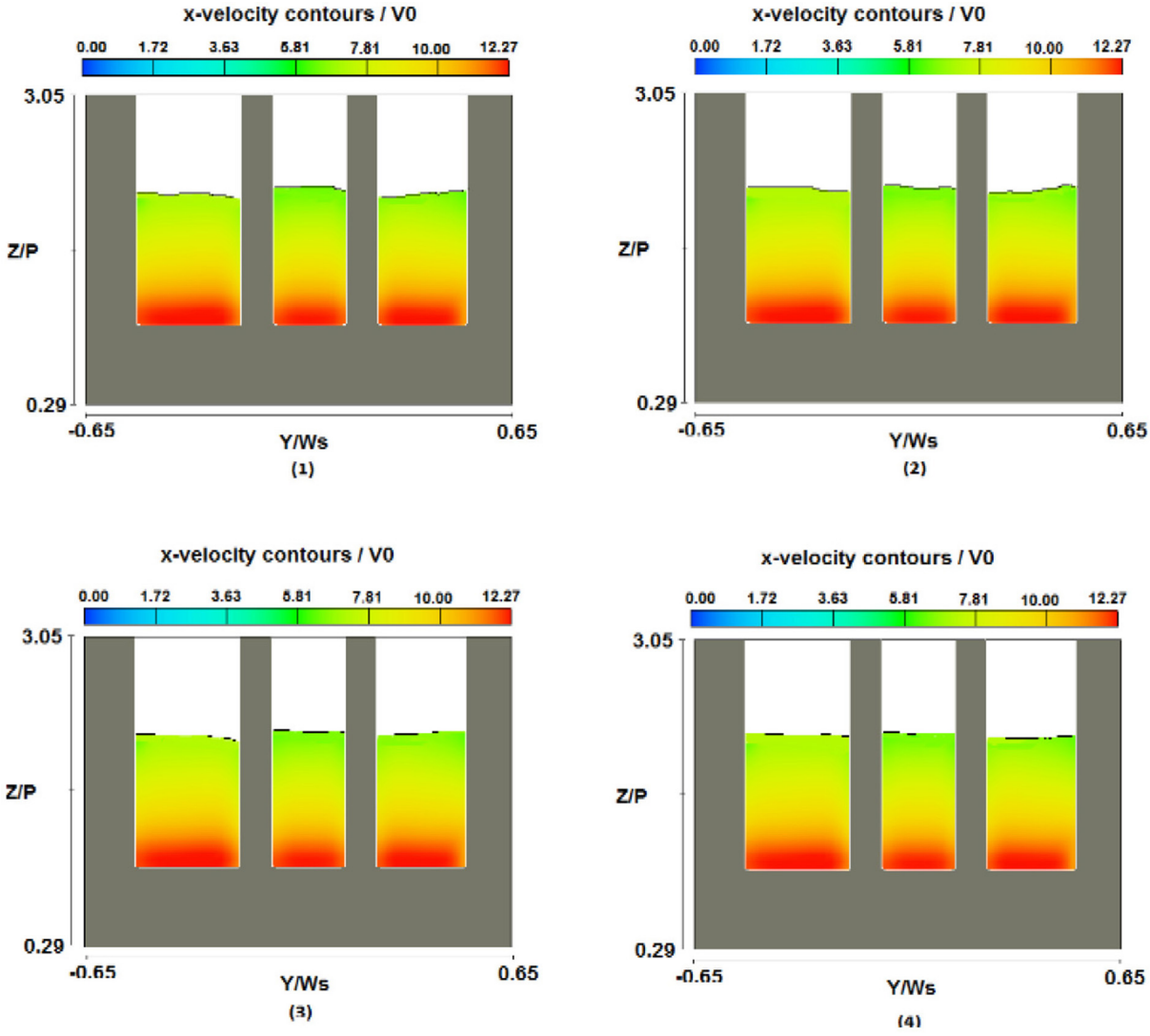

Fig. 30. Cross-section of the flow through the spillway for different vertical inclinations of the piers.

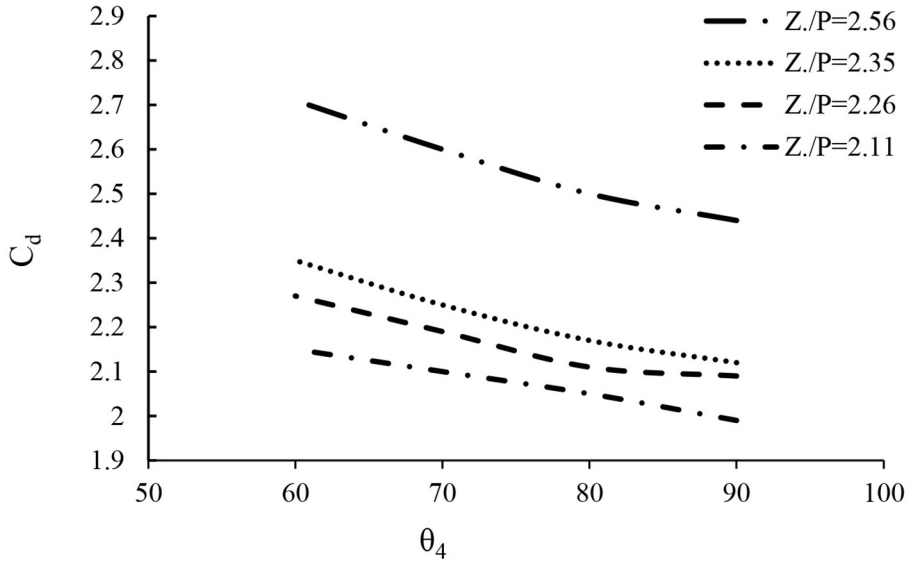

Fig. 31. Discharge coefficient of the spillway for different vertical inclinations of the piers.

4 Conclusion

The present study was performed to illustrate the effect of using guide wall and pier with different geometries on the hydraulic behavior of the flow over a spillway. The performance of the CFD simulations with the selected grid resolution was examined and validated by comparing the results of the simulation with the experimental data for vertical piers inclination and initial geometry of the guide walls. Generally, the numerical results were found to be in good agreement with the experimental data, with an average relative deviation of less than 10%. Different scenarios were numerically simulated to optimize the geometry of the guide walls and piers over the spillway in different hydraulic conditions. Results showed that the vertical inclination of the guide walls and piers was the main affecting factor in the approach flow condition through the spillway. In this study, a 44% increment of the vertical inclination of the left guide wall resulted in a 43% turbulence energy reduction and 13% discharge coefficient increase. By a 28% increase in the vertical inclination of piers, flow behavior became more uniform and discharge coefficient increased by 11%. Moreover, the results of this study showed that the optimal values of the straight length and horizontal inclination of guide wall were affected by the topography of the approach channel and the angle between axis of the approach channel and that of the spillway. In general, increasing the straight length of the guide wall leads to reduction of the average velocity and turbulence energy in the approach channel.

The authors would like to thank the Hydraulic Structures Division of the Water Research Institute for their kind cooperation in using the experimental data.

References

1. C.L. Wu, K.W. Chau, C. Fan, J. Hydrology **389**, 146 (2010).
2. X.Y. Chen, K.W. Chau, A.O. Busari, Eng. Appl. Artif. Intell. **46**, 258 (2015).
3. R. Taormina, K.W. Chau, B. Sivakumar, J. Hydrology **529**, 1788 (2015).
4. W.C. Wang, K.W. Chau, D.M. Xu, L. Qiu, C.C. Liu, Water Resour. Manag. **31**, 461 (2017).
5. J.B. Wang, H.C. Chen, Water Sci. Eng. **3**, 67 (2010).
6. R. Roshan, H. Sarkardeh, A.R. Zarrati, *Vortex study on a hydraulic model of Godar-e-Landar Dam and hydropower plant*, in *Computational Methods in Multiphase Flow V*, edited by A. Mammoli, *WIT Transactions on Engineering Sciences*, Vol. **63** (WIT Press, 2009) pp. 217–225, https://doi.org/10.2495/MPF090191.
7. K. Safavi, A.R. Karaminejad, H. Jamali, H. Sarkardeh, A.R. Zarrati, *Hydraulic design of a multi-level intake structure*, in *Advances in Water Resources and Hydraulic Engineering* (Springer, Berlin, Heidelberg, 2009) pp. 2064–2068.
8. R. Roshan, H.Md. Azamathulla, M. Marosi, H. Sarkardeh, H. Pahlavan, A. Ab Ghani, J. Dams Reserv. **20**, 131 (2010).
9. S.R. Khodashenas, R. Roshan, H. Sarkardeh, H.Md. Azamathulla, Dam Eng. **21**, 131 (2010).
10. R. Roshan, A.R. Karaminejad, H. Sarkardeh, E. Jabbari, A.R. Zarrati, *Design of Spillway Bucket for Kuhrang III Dam by Using a Physical Model*, in *International Symposium on Hydraulic Physical Modeling and Field Investigation (ISHPF 2010)*, China (2010).

11. M. Jorabloo, M. Abdolahpour, R. Roshan, H. Sarkardeh, *A techno-economical view on energy losses at hydropower dams (case study of Karun III Dam and Hydropower Plant)*, in *Computational Methods in Multiphase Flow VI*, Vol. **70**, (2011) p. 253.
12. S.M. Amiri, A.R. Zarrati, R. Roshan, H. Sarkardeh, Proc. Inst. Civ. Eng. Water Manag. **164**, 193 (2011).
13. S.M. Taghvaei, R. Roshan, K. Safavi, H. Sarkardeh, Int. J. Phys. Sci. **7**, 5069 (2012).
14. H. Sarkardeh, E. Jabbari, A.R. Zarrati, S. Tavakkol, Proc. Inst. Civ. Eng. Water Manag. **167**, 356 (2013).
15. M.R. Khanarmuei, H. Rahimzadeh, H. Sarkardeh, Modares Mech. Eng. **14**, 35 (2014) (in Persian).
16. M. Azarpira, H. Sarkardeh, S. Tavakkol, R. Roshan, H. Bakhshi, Sadhana **39**, 1201 (2015).
17. M. Mardani, H. Rahimzadeh, H. Sarkardeh, Modares Mech. Eng. **15**, 31 (2015) (in Persian).
18. M. Marosi, M. Ghomeshi, H. Sarkardeh, Sadhana **40**, 1373 (2015).
19. O. Nazari, E. Jabbari, H. Sarkardeh, Int. J. Civ. Eng. Trans. A Civ. Eng. **13**, 45 (2015).
20. H. Sarkardeh, M. Marosi, R. Roshan, Int. J. Energy Environ. **6**, 597 (2015).
21. M.R. Khanarmuei, H. Rahimzadeh, A.R. Kakuei, H. Sarkardeh, Sadhana **41**, 1055 (2016).
22. F. Kazemi, S.R. Khodashenas, H. Sarkardeh, Int. J. Civ. Eng. **14**, 13 (2016).
23. H. Sarkardeh, Chin. J. Mech. Eng. **30**, 1017 (2017).
24. M. Monshizadeh, A. Tahershamsi, H. Rahimzadeh, H. Sarkardeh, Int. J. Civ. Eng. (2017) `https://doi.org/10.1007/s40999-017-0266-8`.
25. H. Rahimzadeh, J. Yazdi, H. Sarkardeh, Dam Eng. **21**, 171 (2010).
26. M. Jorabloo, R. Maghsoodi, H. Sarkardeh, J. Am. Sci. **7**, 931 (2011).
27. R. Maghsoodi, M.S. Roozgar, H. Sarkardeh, H.Md. Azamathulla, Int. J. Model. Simul. **32**, 237 (2012).
28. H. Rahimzadeh, R. Maghsoodi, H. Sarkardeh, S. Tavakkol, Eng. Appl. Comput. Fluid Mech. **6**, 100 (2012).
29. R. Maghsoodi, M.S. Roozgar, K.W. Chau, H. Sarkardeh, Dam Eng. **23**, 53 (2012).
30. H. Sarkardeh, A.R. Zarrati, E. Jabbari, M. Marosi, Eng. Appl. Comput. Fluid Mech. **8**, 598 (2014).
31. B. Khadem Rabe, S.H. Ghoreishi Najafabadi, H. Sarkardeh, Proc. Inst. Civ. Eng. Water Manag. **171**, 18 (2018).
32. S.A.H. Sajjadi, S.H. Sajjadi, H. Sarkardeh, Int. J. Civ. Eng. **16**, 155 (2018).
33. H. Sarkardeh, Meccanica **52**, 3629 (2017).
34. B. Khadem Rabe, S.H. Ghoreishi Najafabadi, H. Sarkardeh, Curr. Sci. **113**, 141 (2017).
35. F. Tajabadi, E. Jabbari, H. Sarkardeh, Eur. Phys. J. Plus **133**, 10 (2018).
36. F. Naseri, H. Sarkardeh, E. Jabbari, Acta Mech. (2018) `https://doi.org/10.1007/s00707-017-2069-z`.
37. X.P. Jian, J. Hebei, Inst. Archit. Sci. Technol. **22**, 33 (2005).
38. L.F. Hua, X.H. Nan, J. Water Resour. Archit. Eng. **1**, 21 (2003).
39. R. Martinerie, J. Boillat, A. Schleiss, A.P. Rizi, A. Wohnlich, *Experimental Study of the Gated Spillway of the Shahryar Dam in Iran*, in *Proccedings of the Congress-International Association for Hydraulic Research*, Vol. **32** (2007) p. 691.
40. S.D. Kim, H.J. Lee, S.D. An, Int. J. Phys. Sci. **5**, 774 (2010).
41. H. Rahimzadeh, M. Abdolahpour, R. Roshan, H. Sarkardeh, Dam Eng. **22**, 293 (2012).
42. A. Parsaie, A.H. Haghiabi, A. Moradinejad, Sustain. Water Resour. Manag. **1**, 245 (2015).
43. S. Dehdar-Behbahani, A. Parsaie, Alex. Eng. J. **55**, 467 (2016).
44. Water Research Institute (WRI), *Physical Model Study of Jareh Dam*, Technical Report (2010).
45. Q. Chen, G. Dai, H. Liu, J. Hydraul. Eng. **128**, 683 (2002).
46. D.G. Kim, J.H. Park, KSCE J. Civ. Eng. **9**, 161 (2005).
47. A.S. Ramamurthy, S.S. Han, P.M. Biron, J. Comput. Civ. Eng. **27**, 282 (2012).
48. US Army Engineer, *Waterways Experiment Station*, (1952) Hydraulic Design Criteria and subsequent editions.